applied sciences

MDPI

Article

Research on Construction Sequences and Construction Methods of the Small Clear-Distance, Double-Arch Tunnel under an Asymmetrical Load

Shan Wu [1], Jian Wu [1,2] and Dunwen Liu [1,*]

[1] School of Resources and Safety Engineering, Central South University, Changsha 410083, China; 215512141@csu.edu.cn (S.W.); 215512132@csu.edu.cn (J.W.)
[2] Road & Bridge South China Engineering Co., Ltd., Zhongshan 528403, China
* Correspondence: dunwen@csu.edu.cn

Abstract: A small clear-distance, double-arch tunnel under an asymmetrical load combines the characteristics of small clear-distance, tunnels and double-arch tunnels, and the influence of an asymmetrical terrain must be considered. Its construction stability is a problem worth studying. This paper used the Wengcun tunnel as the engineering background. Midas/GTS finite element analysis software was used to study the effects of eight excavation sequences and two excavation methods on tunnel stability. The results showed that the deformation and force of the tunnel were asymmetric under the asymmetrical terrain. Both middle partition walls were deformed towards the shallowly buried side, and the shallowly buried side was deformed to a greater extent. Excavating shallow side tunnels first can effectively mitigate the impact of asymmetric terrain. The arch settlement of the Center Diaphragm Excavation Method is 1.33 cm, which is smaller than the three-step excavation method of 1.48 cm; however, this difference is not significant. The Three-bench Excavation Method was more efficient. Based on the conclusion of a numerical simulation, the construction site adopted the construction sequence of excavating the shallowly buried side tunnel first and adjusted the excavation method to the Three-bench Excavation Method.

Keywords: small clear-distance tunnel; double-arch tunnel; asymmetrical load; construction sequences; construction methods; numerical simulation

Citation: Wu, S.; Wu, J.; Liu, D. Research on Construction Sequences and Construction Methods of the Small Clear-Distance, Double-Arch Tunnel under an Asymmetrical Load. *Appl. Sci.* **2023**, *13*, 8242. https://doi.org/10.3390/app13148242

Academic Editor: Daniel Dias

Received: 15 June 2023
Revised: 8 July 2023
Accepted: 11 July 2023
Published: 16 July 2023

1. Introduction

In recent years, the construction site requirements of mountain tunnels have become increasingly stringent due to route planning and topography. Due to the small footprint of the small clear-distance tunnel, it has been widely used in urban and mountain tunnels [1,2]. During the construction process, it is necessary to ensure the stability of the intermediate rock mass. Another similar type is the double-arch tunnel. The two adjacent tunnels are connected by a middle partition wall [3,4]. These two types of tunnels are different from ordinary tunnels in that they are affected by mutual disturbances between neighbors. Therefore, the safety of their construction cannot be ignored.

Research on double-arch tunnels and small clear-distance tunnels has mainly focused on theoretical analysis, field tests, model tests, and numerical simulations. Regarding theoretical analysis, Fu et al. [5] proposed an analytical solution, considering the interaction between tunnels for the stress and displacement problem of parallel double tunnels. Li et al. [6] studied the effect of different distances as well as the surface slope on the surrounding rock pressure of an asymmetrical load on a small clear-distance tunnel. Yang et al. [7] proposed an analytical solution to determine the internal forces of a shallow-buried, double-continuous arch tunnel support structure under symmetric loading. Combining the force method with the unbalanced force transformation method, Hu et al. [8] proposed an internal force calculation method for Double-O-tube lining. In terms of field measurement, Yao et al. [9] conducted on-site monitoring of the double-arch tunnel at Zipuiping and identified the upper and lower step intersection areas and the middle partition wall as weak locations. Wu et al. [10] derived from the site geology of a tunnel with a double-arch tunnel that the over-excavation problem occurs mainly in the connection area between the middle guide tunnel and the main tunnel. Yan et al. [11] conducted on-site monitoring of a double-arch tunnel and showed that the tunnel deformation and forces are directly related to its location and geological and construction process. Lai et al. [12] conducted an overall inspection of a double-arch tunnel and found that the tunnel lining cracks were mainly located in the middle partition wall, the side wall, and on the top of the arch. Yuan et al. [13] conducted a detailed monitoring and data analysis for a double-arch tunnel and then provided design and construction recommendations based on this. In terms of model tests, Lei et al. [14] developed an experimental model of a tunnel with a small clear distance under asymmetric loading and used the model to analyze the damage mechanism of the surrounding rock under asymmetrical topography. Jiang et al. [15] carried out a large shaking table test to investigate the effects of the seismic wave type and acceleration excitation peak on the strain response pattern of shallowly buried asymmetrical loading small clearance tunnel lining. Li et al. [16] conducted physical model tests and numerical simulations of the Great Wall Ridge Tunnel to gain a comprehensive understanding of the deformation law of the shallow-buried, double-arch tunnel. Yang et al. [17] used strain gauges to monitor the longitudinal deformation of the pipe roof at the entrance of a shallow-buried continuous arch tunnel and found that the double-layer pipe roof could play a good role in limiting the surface deformation. Based on indoor model tests and numerical simulation, Liu et al. [18] studied the tunnel profile displacement and stress and pressure arch distribution law of the surrounding rock during the excavation of the loess continuous arch tunnel.

On-site monitoring can only be performed for a particular project, and physical models are costly to produce. Numerical simulation was widely used because of its convenience and low cost in recent years. Wang et al. [19] used numerical simulation to study the mechanical response of a small clear-distance tunnel in Xiamen and compared the mechanical response of the tunnel under different excavation methods, different feeds, and different surrounding rock grades. Ng et al. [20] investigated the interaction of a large-section parallel tunnel in hard clay soils by building a three-dimensional finite element model. Zhang et al. [21] used Ansys finite element software to study the excavation sequence problem of a shallow-buried asymmetrical loading small clearance tunnel under different conditions and came up with a reasonable excavation sequence for different spacing, slope, and burial depth. Xu et al. [22] proposed a hybrid construction method for a small clear-distance tunnel and compared it with the CRD construction method using numerical simulation to verify the effectiveness of the hybrid construction method. Wang et al. [4] conducted a numerical simulation of the whole process for a shallow-buried, large-span, double-arch tunnel under the faulted and broken zone of the highway. Soliman et al. [23] analyzed the interaction of the two tunnel tubes using the finite element method to derive the relative change processes of stress and strain. Bai et al. [24] analyzed the construction process of the double-arch tunnel using the numerical simulation model as well as on-site monitoring and found the deformation pattern of the support structure. Yao et al. [25] studied the effect of double-arch tunnels on transmission tower foundations via numerical simulation and compared the mechanical correspondence of tower foundations under different construction schemes and different construction sequences.

However, in the existing studies, most of the scholars have studied only one type of small clear-distance tunnel or double-arch tunnel. There is a lack of research on small clear-distance, double-arch tunnels, especially in asymmetrical terrain and fractured surrounding rock conditions. Therefore, in this paper, we used numerical simulation to study the behavior of the construction mechanics of a small clear-distance, double-arch tunnel under an asymmetrical load. The aim is to explore its reasonable construction sequence as well as construction methods. The findings of the study can provide references for similar projects.

2. Project Overview

This project is based on the Wengcun tunnel, a separate tunnel on the Guilin to Liuzhou expressway in Guangxi. It is located in a section of the highway's reconstruction and expansion, as shown in Figure 1a. The left tunnel section spans from ZK1182+340 to ZK1182+825, with a length of 485 m and a maximum burial depth of approximately 92 m. The right tunnel section spans from YK1182+410 to YK1182+836, with a length of 426 m and a maximum burial depth of 79 m. The distance between the left and the right tunnel is approximately 18 m, making it a small clear-distance, double-arch tunnel. The actual topographical overview of the mountainous area where the tunnel is located is illustrated in Figure 1b.

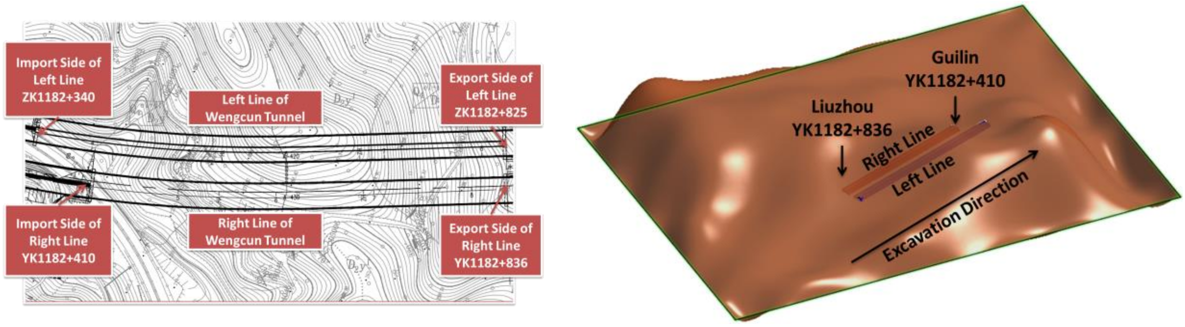

(**a**) (**b**)

Figure 1. Overview of the mountainous area where the tunnel is located: (**a**) plan view; (**b**) actual terrain.

Taking into account the construction access conditions and land acquisition and demolition situation, the plan is to start excavation from the Liuzhou end (YK1182+836). The YK1182+450 cross-section of the tunnel profile is selected as the focus of this study, and its profile is shown in Figure 2. The geological formation consists of strongly to moderately weathered argillaceous sandstone that is interbedded with sandstone. The surrounding rock is broken and belongs to the V surrounding rock.

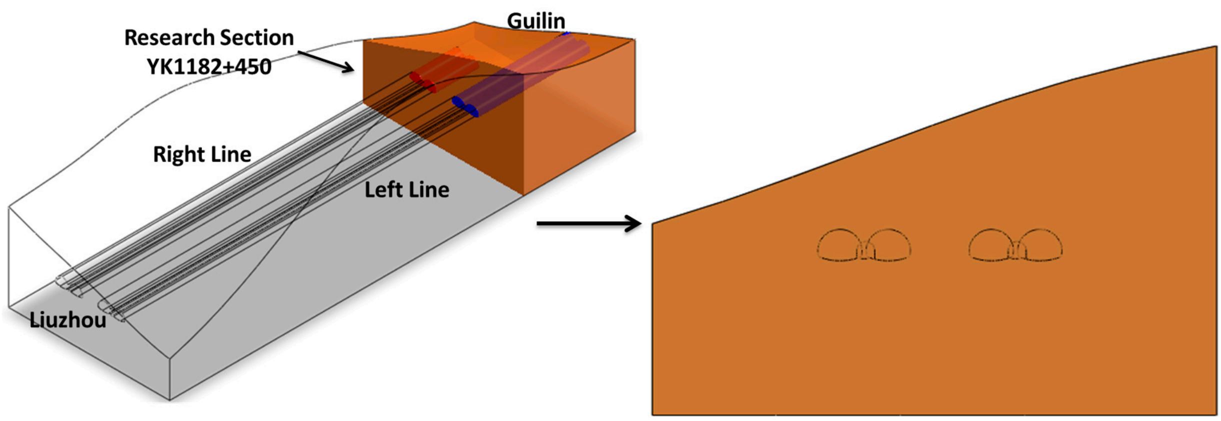

Figure 2. Research section YK1182+450.

3. Numerical Model

3.1. Model Building

The excavation sequence and the excavation method for the small clear-distance, double-arch tunnel are critical issues in this project. Based on the typical cross-section of YK1182+450, a two-dimensional numerical model was established as shown in Figure 3. In the tunnel support system, the initial lining is the main support structure. Therefore, the influence of the secondary lining on the tunnel is not considered throughout the entire simulation process.

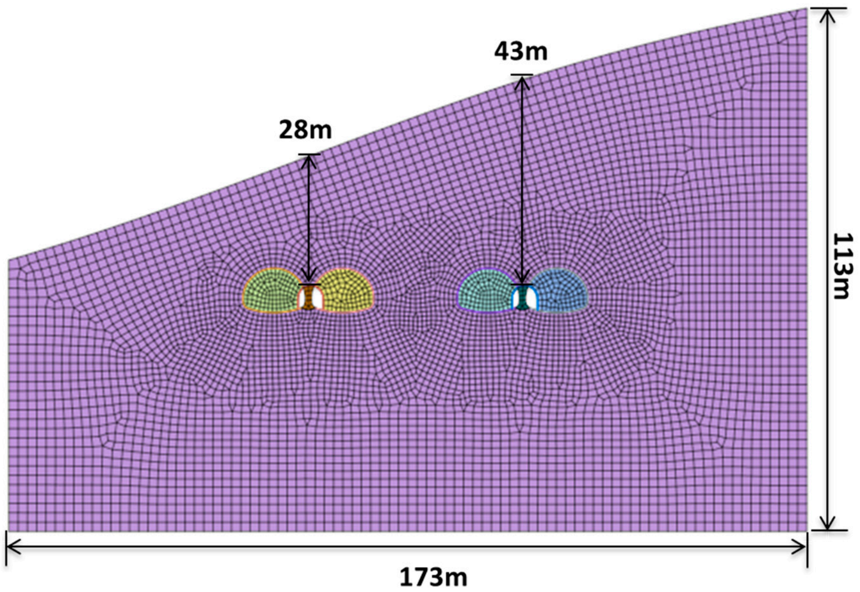

Figure 3. Numerical model of YK1182+450 cross-section.

The modeling was carried out using the finite element software Midas/GTS. The model has a horizontal dimension of 173 m and a vertical dimension of 113 m. The upper boundary was set as a free boundary to match the actual ground surface. The left and right tunnel lines have burial depths of approximately 43 m and 28 m, respectively. The distances between the left and right boundaries of the model and the tunnel are about 50 m, and they are subjected to horizontal constraints. The lower boundary of the model is about 50 m away from the tunnel and is subjected to vertical and horizontal constraints. The failure criterion for the surrounding rock was the Mohr–Coulomb criterion, while the concrete material was modeled as a linear elastic material. Plane strain elements were used to simulate the surrounding rock and the middle partition walls, while beam elements were used to simulate the initial support.

3.2. Model Parameters

Based on a comprehensive consideration of the site geological survey and reference values from the related specifications [25] regarding rock mass and structural parameters, the physical and mechanical parameters for the rock mass and support system are shown in Table 1.

Table 1. Physical and mechanical parameters for rock mass and support system.

Category	Severe (kN/m^3)	Elastic Modulus (GPa)	Poisson's Ratio	Friction Angle (°)	Cohesion (kPa)	Property
Level V Rock Mass	17	1	0.37	20	100	Plane Strain
Initial Support	23	27.2	0.2	/	/	Beam
Middle Partition Wall	25	32.5	0.2	/	/	Plane Strain

3.3. Simulation Schemes

During the numerical simulation process, it is important to first determine the excavation sequence. When the optimal excavation sequence is established, the excavation method can be discussed. To facilitate analysis, the four tunnels can be designated as Tunnel 1, Tunnel 2, Tunnel 3, and Tunnel 4, in the order from shallow to deep. The middle partition wall on the shallow side can be referred to as the middle partition wall 1, and the one on the deep side is the middle partition wall 2. According to the site information, construction work on the two middle partition walls was completed before tunnel excavation.

3.3.1. Simulation Scheme of Excavation Sequence

During the process of simulating the excavation sequence, the focus should be on the impact of the sequence on the surrounding rock and support structures. Therefore, the influence of excavation methods is not considered. The excavation of the tunnels is performed using the full-face method uniformly. With the completion of the excavation for the four tunnels, a total of eight excavation sequences have been simulated, as shown in Table 2.

Table 2. Construction steps for different excavation sequences.

Excavation Sequence	Construction Process
1234	Excavation 1 → Support 1 → Excavation 2 → Support 2 + Removal of the middle partition wall support 1 → Excavation 3 → Support 3 → Excavation 4 → Support 4 → Removal of the middle partition wall support 2
1243	Excavation 1 → Support 1 → Excavation 2 → Support 2 + Removal of the middle partition wall support 1 → Excavation 4 → Support 4 → Excavation 3 → Support 3 + Removal of the middle partition wall support 2
2134	Excavation 2 → Support 2 → Excavation 1 → Support 1 + Removal of the middle partition wall support 1 → Excavation 3 → Support 3 → Excavation 4 → Support 4 → Removal of the middle partition wall support 2
2143	Excavation 2 → Support 2 → Excavation 1 → Support 1 + Removal of the middle partition wall support 1 → Excavation 4 → Support 4 → Excavation 3 → Support 3 + Removal of the middle partition wall support 2
3412	Excavation 3 → Support 3 → Excavation 4 → Support 4 + Removal of the middle partition wall support 2 → Excavation 1 → Support 1 → Excavation 2 → Support 2 + Removal of the middle partition wall support 1
3421	Excavation 3 → Support 3 → Excavation 4 → Support 4 + Removal of the middle partition wall support 2 → Excavation 2 → Support 2 → Excavation 1 → Support 1 + Removal of the middle partition wall support 1
4312	Excavation 4 → Support 4 → Excavation 3 → Support 3 + Removal of Intermediate Wall Support 2 → Excavation 1 → Support 1 → Excavation 2 → Support 2 + Removal of the middle partition wall support 1
4321	Excavation 4 → Support 4 → Excavation 3 → Support 3 + Removal of Intermediate Wall Support 2 → Excavation 2 → Support 2 → Excavation 1 → Support 1 + Removal of the middle partition wall support 1

3.3.2. Simulation Scheme of Excavation Method

After determining the optimal excavation sequence, the selection of excavation methods should be carried out according to the optimal excavation sequence. The commonly used excavation methods for double-arch tunnels under V-grade surrounding rocks are the medium-guide cavern method and the three-guide cavern method, etc. Based on this, in the present project conditions, the Three-bench Excavation Method and Center Diaphragm Excavation Method are compared, and their construction steps are shown in Figure 4. After the construction of one side of the double-arch tunnel is completed, the temporary support will be removed.

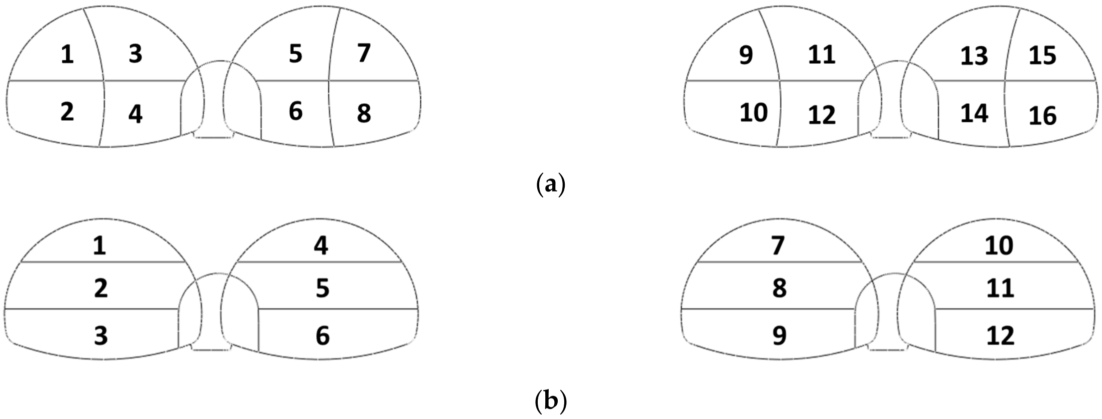

Figure 4. Tunnel excavation methods: (**a**) Center Diaphragm Excavation Method; (**b**) Three-bench Excavation Method.

4. Results and Discussion

4.1. Analysis of Excavation Sequence

4.1.1. Deformation Analysis

(1) Deformation analysis of the surrounding rock and tunnel

The deformation patterns of the surrounding rock under different excavation sequences were generally consistent. Taking the excavation sequence of "1234" for example, the vertical deformation cloud map and horizontal deformation cloud map are shown in Figures 5 and 6, respectively. From Figure 5, it could be observed that the vertical deformation of the surrounding rock was mainly concentrated at the arch top and the arch bottom, exhibiting a form of settlement and uplift. From Figure 6, it could be seen that the horizontal deformation of the surrounding rock was mainly concentrated at the junction between the tunnel and the middle partition wall, as well as the sidewall locations, exhibiting a converging pattern towards the interior of the tunnel. Overall, both the vertical and horizontal deformations were asymmetric, which was a result of an asymmetrical topography [26]. Additionally, due to the characteristics of the double-arch tunnel, both the vertical and horizontal deformations of the surrounding rock tended to concentrate toward the middle partition wall.

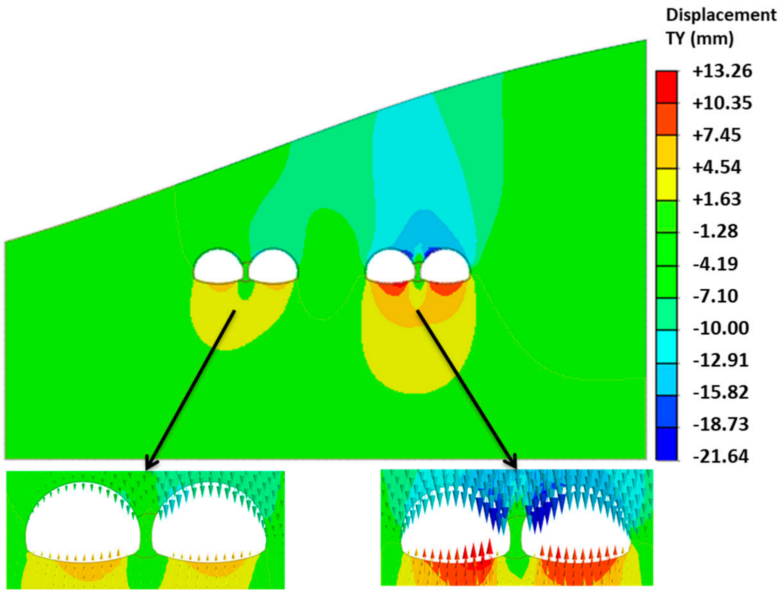

Figure 5. Vertical displacement cloud map.

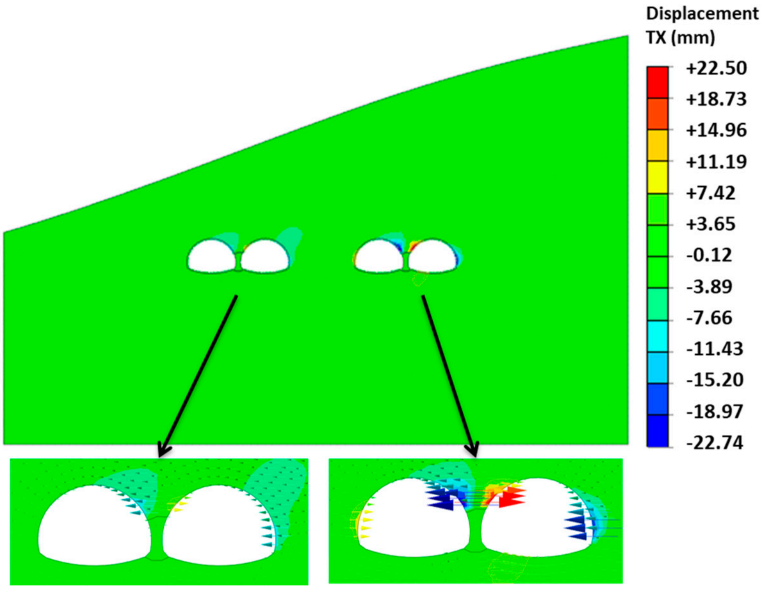

Figure 6. Horizontal displacement cloud map.

After construction, the maximum deformation occurred in the more deeply buried double-arch tunnel. Among them, the maximum settlement deformation was observed at the left upper arch shoulder of Tunnel 4, marked as point A. The maximum uplift was observed at the right lower side of Tunnel 3, marked as point B. The maximum horizontal displacement was observed at the right upper arch shoulder of Tunnel 3, marked as point C. The locations of points A, B, and C are shown in Figure 7.

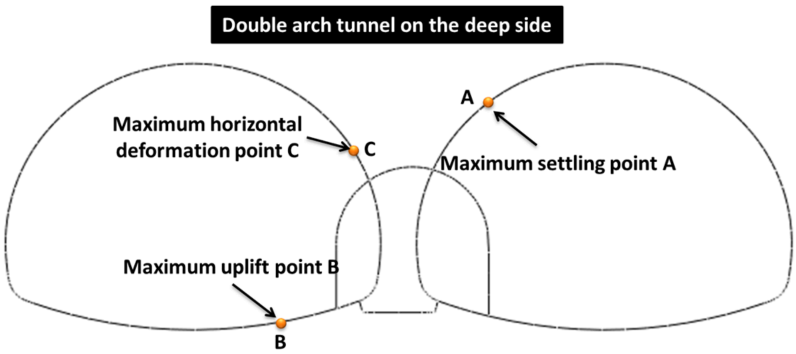

Figure 7. Measurement points of Tunnel 4.

The variation of the deformation indicators at points A, B, and C under different excavation sequences are shown in Figure 8a–c. Overall, the deformation process of the tunnel consisted of two stages: "slow deformation" and "rapid deformation". The "slow deformation" was the disturbance deformation caused by the excavation of surrounding tunnels, while the "rapid deformation" was the direct deformation caused by the excavation of the tunnel itself. According to Figure 8a,b, it could be observed that the final cumulative values of the settlement at the arch top and the uplift at the arch bottom remained around 21 mm and 13 mm, respectively, regardless of the excavation sequence. This indicated that the influence of the excavation sequence on the vertical deformation of the tunnel mainly lay in the difference in the occurrence times of the "slow deformation" and "rapid deformation", while the final cumulative values were relatively similar. According to Figure 8c, it could be seen that the final cumulative values of the horizontal deformation of the tunnel differed to some extent under different excavation sequences. The horizontal deformation under the "1234", "2134", "3412", and "3421" sequences was approximately 22 mm, while it was around 26 mm under the "1243", "2143", "4312", and "4321" sequences. This indicated that the excavation sequence also affected the final value of the horizontal deformation. To better control the horizontal deformation of the tunnel, it was recommended to adopt the "1234", "2134", "3412", and "3421" sequences.

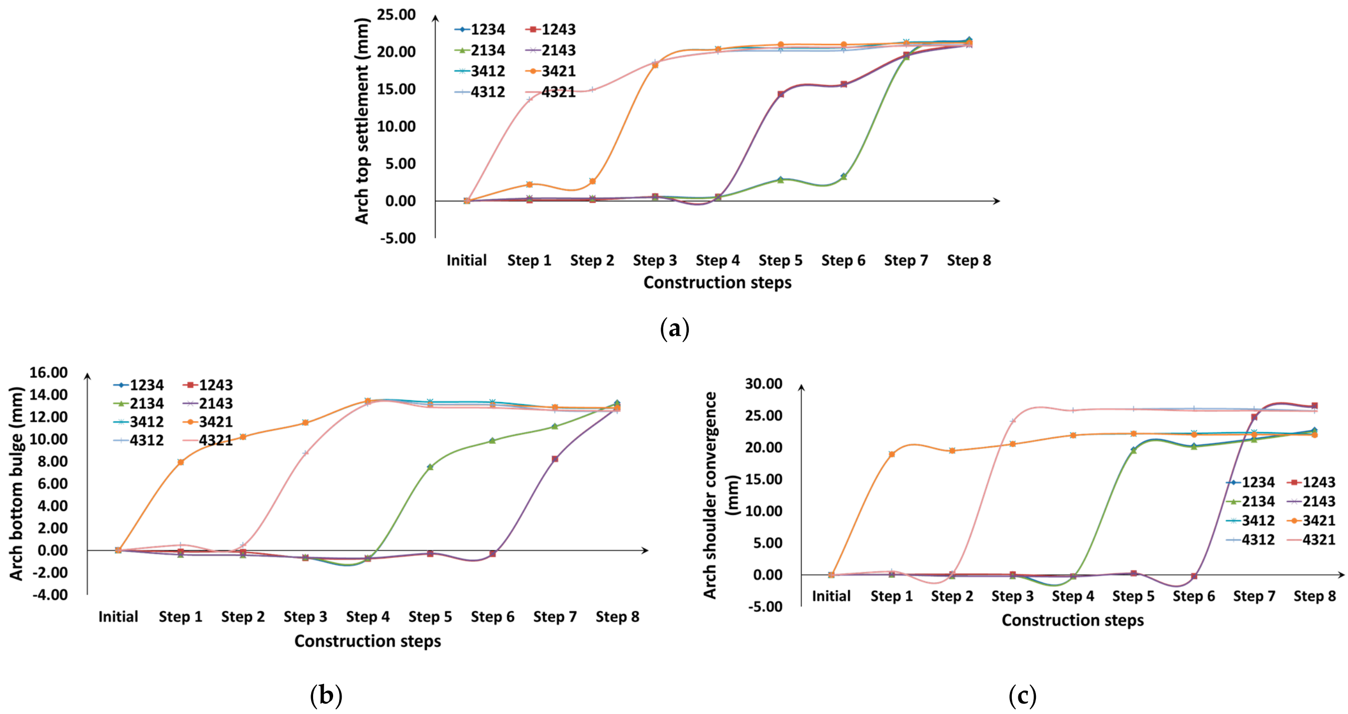

Figure 8. Deformation of measurement points with construction steps: (**a**) measurement point A; (**b**) measurement point B; (**c**) measurement point C.

(2) Tipping analysis of the middle partition wall

The tilting of the middle partition wall was mainly related to its horizontal displacement. Regardless of the excavation sequence, the middle partition walls on the left and right sides would experience tilting deformation, and the maximum deformation would occur at the top of the partition wall [16]. However, different excavation sequences had a certain influence on the tilting displacement of the middle partition wall. For example, when comparing the excavation sequences "1234" and "1243" as shown in Figure 9a,b, it was observed that the maximum horizontal displacement of the middle partition wall 2 was smaller in the "1234" sequence compared to the "1243" sequence. Similarly, when comparing the excavation sequences "1234" and "2134" as shown in Figure 9a,c, it could be seen that the maximum horizontal displacement of the middle partition wall 1 was smaller in the "1234" sequence compared to the "2134" sequence.

Furthermore, from the overall perspective of Figure 9, the tilting amplitude of the middle partition wall 1 was generally greater than that of the middle partition wall 2. This was due to the way the middle partition wall was subjected to forces, as shown in Figure 10. P4 represented the trapezoidal distributed soil pressure acting on the top of the double-arch tunnel. Due to the different surrounding rock pressures, the magnitude of the forces on the supporting structures on both sides was not the same, resulting in P1 > P2. The difference between the two forces caused the middle partition wall to deflect towards the shallow side. In addition, due to the tilting of the top of the middle partition wall, the rock pressure acting on the top of the wall included not only the vertical pressure P5 but also the lateral pressure P3 in the horizontal direction. The size of the top of the middle partition wall was generally much smaller than its burial depth. According to Saint Venant's principle, the trapezoidal load acting on the top of the middle partition wall could be equivalent to a uniformly distributed rectangular load. Among them, P5 did not cause the tilting of the middle partition wall, while P3 caused the deflection towards the deep side. This reduced the tilting amplitude of the middle partition wall towards the shallow side. P3 increased with an increase in burial depth; however, the difference between P2 and P1 did not increase. Therefore, the tilting degree of middle partition wall 1 would be greater than that of middle partition wall 2.

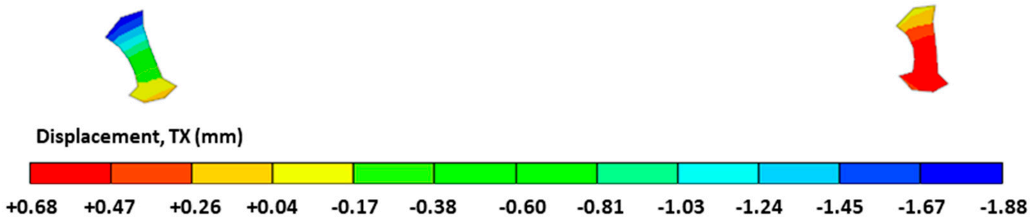

(**a**)

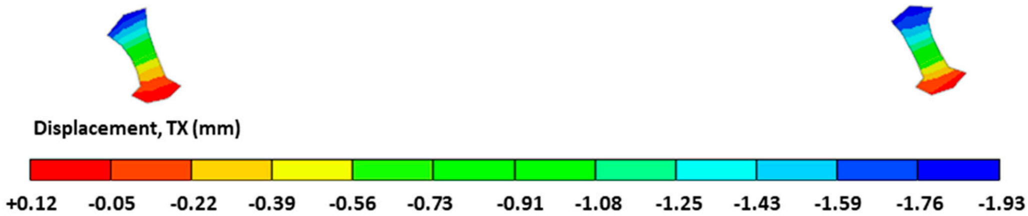

(**b**)

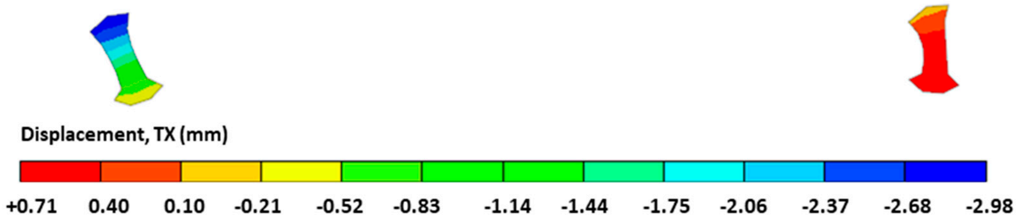

(**c**)

Figure 9. Horizontal deformation of the central partition wall under different excavation schemes: (**a**) excavation sequence of "1234"; (**b**) excavation sequence of "1243"; (**c**) excavation sequence of "2134".

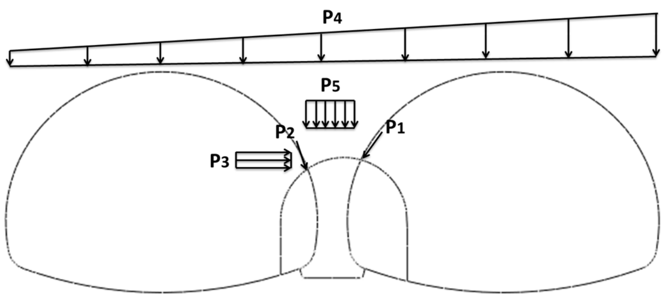

Figure 10. Diagram of the force on the middle partition wall.

The change process of the horizontal deformation of the top of the middle partition walls with the excavation steps under different excavation sequences is shown in Figures 11a and 11b, respectively. The deformation curves of the septum wall fluctuated repeatedly for both the deeply buried side and the shallowly buried side. This indicated that the middle partition walls were subject to frequent disturbances during the construction of the tunnel. First, the horizontal deformation of the top of the partition wall on the shallowly buried side was analyzed, as shown in Figure 11a. It could be seen that the horizontal deformation of "1234", "1243", "3412", and "4312" was smaller. These were compiled into set A. Next, the horizontal deformation of the top of the partition wall on the deeply buried side was analyzed, as shown in Figure 11b. It could be seen that "1234", "2134", "3412", and "3421" were smaller. These were compiled into set B. The intersection of set A and set B was taken, i.e., "1234" and "3412", which had the most balanced control effect on the horizontal deformation of middle partition walls.

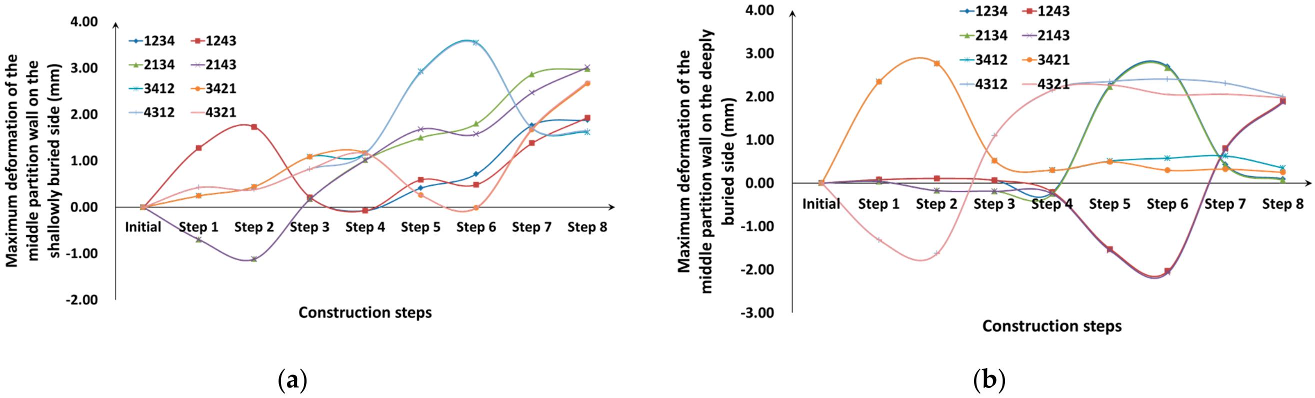

Figure 11. Horizontal deformation curves of the middle partition wall with excavation steps under different excavation sequences: (**a**) the middle partition wall on the shallowly buried side; (**b**) the middle partition wall on the deeply buried side.

4.1.2. Force Analysis

(1) Stress analysis of the support structure

The stresses in the support structure under different excavation scenarios are shown in Figure 12. Regardless of the excavation sequence, the stresses in the support structure of the deeply buried side were generally greater than those in the shallowly buried side. In addition, the stresses in the support structure were greater in the area where the arch shoulder was combined with the middle partition wall. This corresponded to the monitoring results and the fact that spalling and cracking were mostly observed in the combination of the middle partition wall and the arch shoulder. Therefore, in the design and construction process of the double-arch tunnel, the combination of the middle partition wall and the arch shoulder was considered the key control area.

It is worth noting that different excavation sequences had an impact on the location of stress distribution in the support structure. Firstly, let us analyze the stress state of the support structure on the deeply buried side. Taking the two excavation sequences "1234" and "1243" as examples, as shown in Figure 12a,b, it can be observed that the maximum stress of the support structure in the "1234" sequence occurred at Tunnel 3, while the maximum stress of the support structure in the "1243" sequence occurred at Tunnel 4. Secondly, let us analyze the stress state of the support structure on the shallowly buried side of the arch tunnel. Taking the two excavation sequences "1234" and "2134" as examples, as shown in Figure 12a,c, it can be observed that the maximum stress of the support structure in the "1234" sequence occurred at Tunnel 1, while the maximum stress of the support structure in the "2134" sequence occurred at Tunnel 2. This situation was due to the fact that, during the construction of a double-arch tunnel, the later tunnel disturbed the earlier tunnel, thereby increasing the stresses on the support structure of the earlier tunnel.

The maximum stresses of each support structure for different excavation sequences are shown in Table 3. The maximum stresses in the support structure of the double-arch tunnel on the shallow-buried side for different excavation sequences are shown in Figure 13a; moreover, for the deeply buried side, they are shown in Figure 13b. Since the stress in the support structure on the deeply buried side was high, the first consideration was to make the force state of the support structure on the deeply buried side more reasonable. According to Figure 13b, it can be observed that the excavation sequences "1234", "2134", "3412", and "3421" achieved better results; therefore, they were organized into set C.

Then, the focus shifted to making the support structure on the shallow-buried side more reasonable in force. According to Figure 13a, it could be seen that the excavation sequences "1234", "1243", "3412", and "4312" achieved better results; therefore, they were organized into set D. By taking the intersection of set C and set D, it was found that the excavation sequences "1234" and "3412" were optimal. This also indicated that the force magnitude of the support structure was more likely to be influenced by the excavation sequence of the single-lane, double-arch tunnel itself. In other words, the respective excavations of the left-line tunnel and the right-line tunnel had less impact on each other.

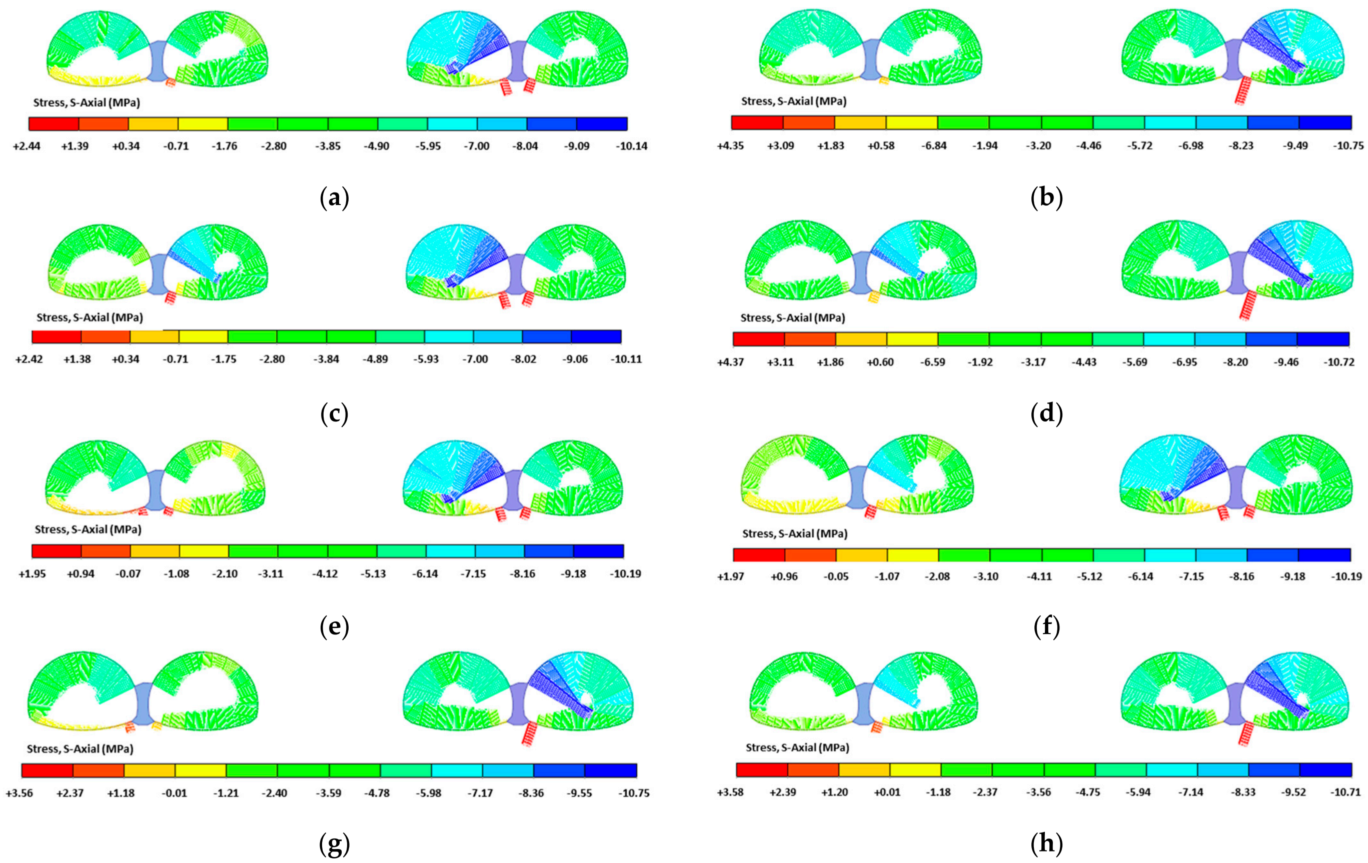

Figure 12. Stress cloud diagram of support structures under different excavation sequences: (**a**) excavation sequence of "1234"; (**b**) excavation sequence of "1243"; (**c**) excavation sequence of "2134"; (**d**) excavation sequence of "2143"; (**e**) excavation sequence of "3412"; (**f**) excavation sequence of "3421"; (**g**) excavation sequence of "4312"; (**h**) excavation sequence of "4321".

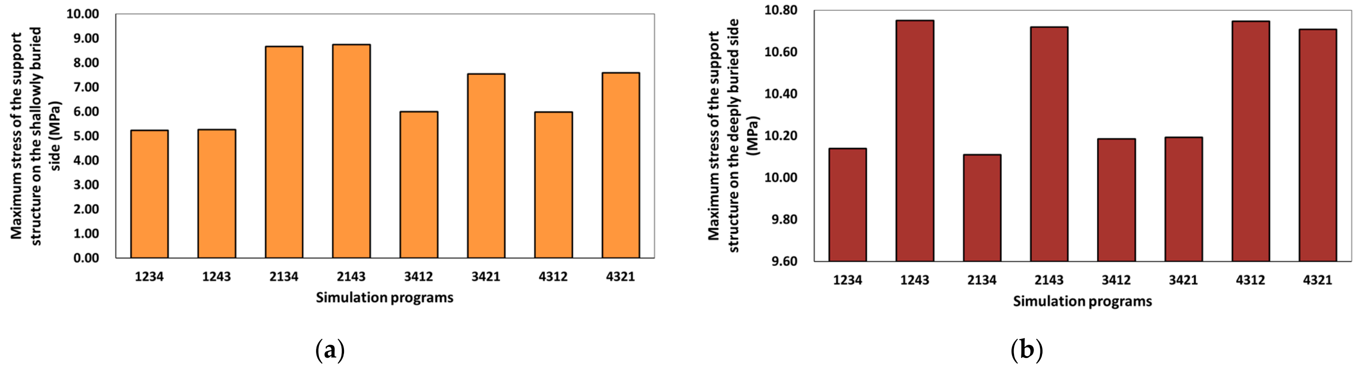

Figure 13. The maximum stress of the left and right lines of the support structure: (**a**) the shallowly buried side; (**b**) the deeply buried tunnel side.

Table 3. The maximum stress of different tunnel support structures.

Excavation Sequence	Tunnel 1 (MPa)	Tunnel 2 (MPa)	The Larger between Tunnel 1 and Tunnel 2 (MPa)	Tunnel 3 (MPa)	Tunnel 4 (MPa)	The Larger between Tunnel 3 and Tunnel 4 (MPa)
1234	5.227	5.106	5.23	10.140	5.544	10.14
1243	5.262	5.145	5.26	5.330	10.750	10.75
2134	3.714	8.666	8.67	10.109	5.524	10.11
2143	3.729	8.746	8.75	5.313	10.719	10.72
3412	5.986	3.760	5.99	10.186	6.000	10.19
3421	3.386	7.539	7.54	10.192	5.886	10.19
4312	5.971	3.788	5.97	5.735	10.747	10.75
4321	3.401	7.585	7.59	5.702	10.708	10.71

(2) Stress analysis of the middle partition wall

The distribution pattern of the main stresses in the middle partition wall under different excavation sequences was similar. Taking the excavation sequence of "1234" as an example, its maximum and minimum principal stresses are shown in Figures 14a and 14b, respectively. It can be seen from Figure 14 that the stress in the middle partition wall on the deep side was greater than that on the shallow side, regardless of the excavation sequence. From the distribution areas of the maximum principal stress and minimum principal stress, the middle partition wall produced a concentrated tensile stress area at its bottom. The compressive stress area of the middle partition wall was mainly concentrated on both sides. Considering the weak tensile properties of concrete, the anchorage at the bottom of the diaphragm wall should have been strengthened in design and construction to prevent its damage due to excessive tensile stresses.

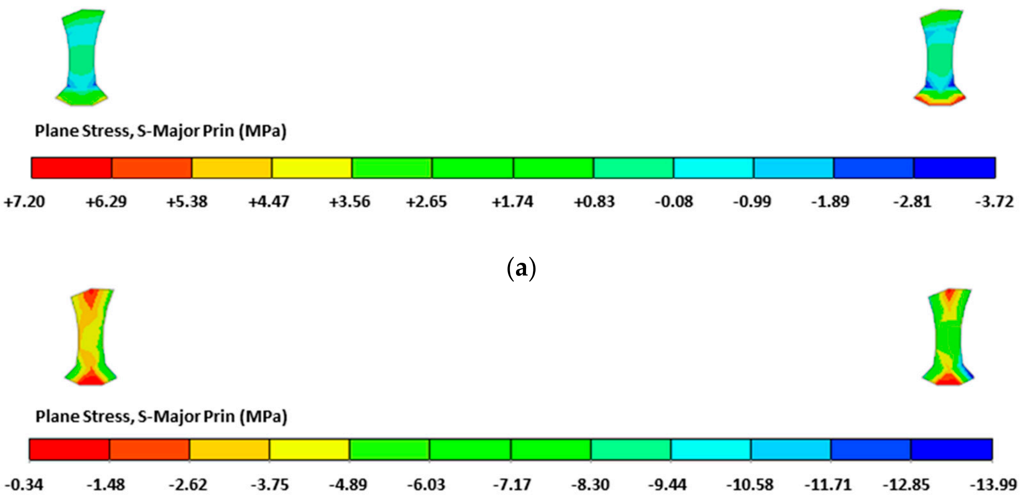

(**b**)

Figure 14. Principal stress of the central partition wall: (**a**) the tensile principal stress; (**b**) the compressive principal stress.

Under different excavation sequences, the maximum tensile principal stress of the middle partition wall on the shallowly buried side and deeply buried side is shown in Figures 15a and 15c, respectively. The maximum compressive principal stress on the shallowly buried side and deeply buried side is shown in Figures 15b and 15d, respectively. Considering the weak tensile properties of concrete, it was important to prioritize the reduction of the tensile stresses experienced by the middle partition wall. Figure 15c illustrates the maximum tensile stresses in the middle partition wall on the deeply buried side under different excavation sequences. Among the four excavation sequences of "1234", "2134", "3412", and "3421", better results were achieved, and they were organized into set E. Regarding the maximum tensile stress of the middle partition wall on the shallowly buried side, as shown in Figure 15a, the four excavation sequences of "1234", "1243", "3412", and "4312" achieved better results and were organized into set F. By taking the intersection of set E and set F, it was determined that the two excavation sequences "1234" and "3412" were the best in terms of reducing the tensile stresses on the middle partition wall. This finding aligned with the excavation order obtained after analyzing the force state of the support structure.

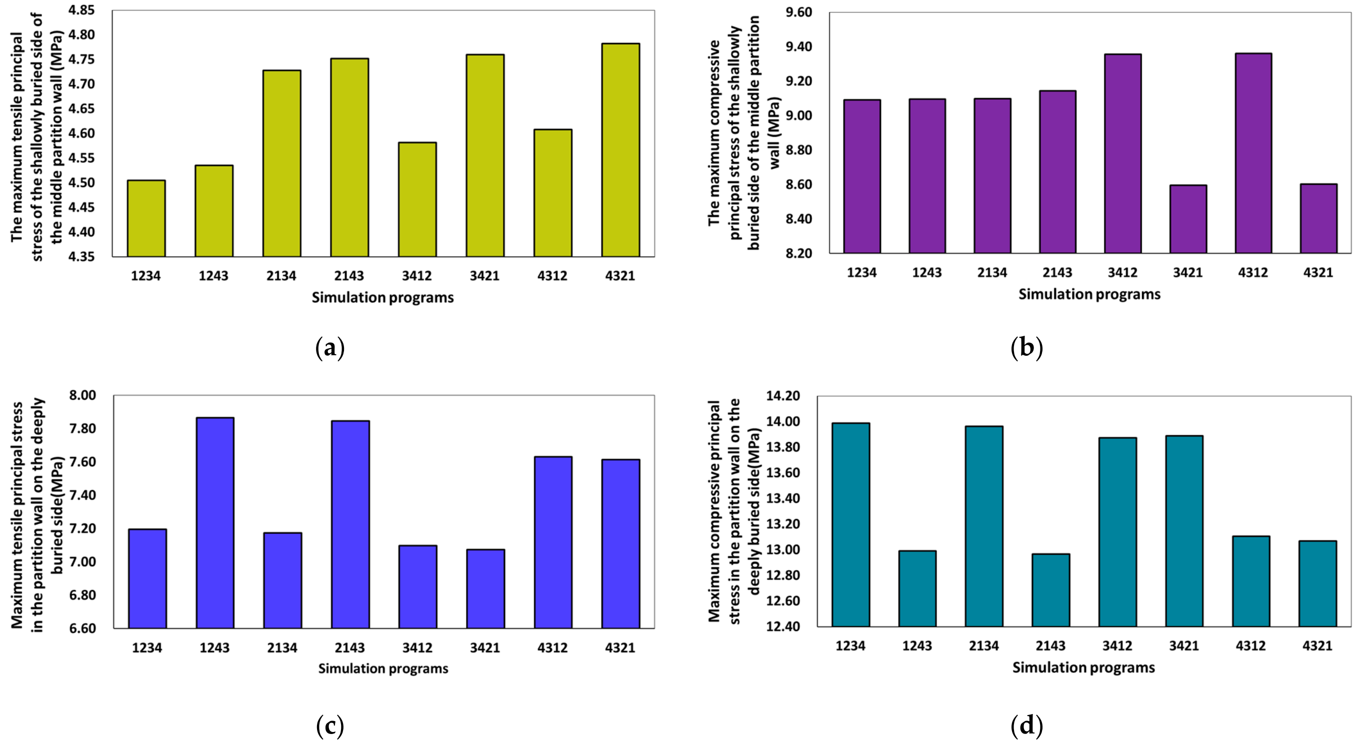

Figure 15. The maximum value of the principal stress in the middle partition wall under different excavation sequences: (**a**) the maximum value of the tensile principal stress on the shallowly buried side; (**b**) the maximum value of compressive principal stress on the shallowly buried side; (**c**) the maximum value of the tensile principal stress on the deeply buried side; (**d**) the maximum value of the compressive principal stress on the deeply buried side.

4.1.3. Determination of Excavation Sequence

From the above data, it was clear that, during the construction of a small clear-distance, double-arch tunnel under an asymmetrical load, different excavation sequences had a greater impact on the horizontal deformation than on the vertical deformation. In the asymmetrical terrain, the deeply buried side of the tunnel was under greater pressure from the surrounding rock. Therefore, it was important to consider reducing the load on the deeply buried side of the support structure first. If the deeply buried side of the tunnel was excavated first, the later tunnel would cause a secondary disturbance to the support structure already erected on the deeply buried side, increasing the force on the deeply buried side. Conversely, if the shallow side of the tunnel was excavated first, the support structure on the deeply buried side would not be disturbed, which would be more beneficial to the safety of the tunnel. This was also consistent with the findings of Zhao et al. [27].

The numerical simulation results showed that there was little difference between the two excavation sequences "1→2→3→4" and "3→4→1→2". This indicated that the force state of the support structure was more likely to be influenced by the excavation sequence of the double-arch tunnel itself, rather than the excavation sequence of the left line and the right line. Therefore, the key to the construction sequence was that "Tunnel 2" should be excavated after "Tunnel 1", and that "Tunnel 4" should be excavated after "Tunnel 3". Based on the engineering geological conditions and numerical simulation results, the excavation sequence of either "1→2→3→4" or "3→4→1→2" was recommended.

4.2. Analysis of Excavation Methods

4.2.1. Plastic Zone Analysis

The final equivalent plastic strain distribution of the surrounding rock is shown in Figure 16. The plastic zone of the surrounding rock caused by the two methods of construction was roughly similar and particularly evident on the rock between the arches at the top of the middle partition wall, on both sides of the tunnel, near the foot of the outer arch of the tunnel, and at the bottom of the middle partition wall. This was related to the force form of the double-arch tunnel. The effective plastic strain in the surrounding rock, when excavated using the Center Diaphragm Excavation Method, is shown in Figure 16a. Compared with Three-bench Excavation Method, the distribution characteristics of the plastic zone of the surrounding rock at the top of the center wall were more dispersed and gentle due to the side guide holes and temporary supports, while the radial depth was not large. The effective plastic strain of the surrounding rock when the Three-bench Excavation Method was used for excavation is shown in Figure 16b. It can be seen that the radial depth of the plastic area of the surrounding rock at the top of the middle diaphragm wall under the three-step excavation method was larger. This was because the Three-bench Excavation Method involved excavating from top to bottom, layer by layer, without side guide holes and temporary support. The plastic zone generated in the surrounding rock of the tunnel sidewalls was more pronounced when using the three-step excavation. Numerically, the maximum plastic strain generated by using Center Diaphragm Excavation Method was 4.538×10^{-3}, while the maximum plastic strain generated by using Three-bench Excavation Method was 5.456×10^{-3}, making the Center Diaphragm Excavation Method superior to the Three-bench Excavation Method. The Center Diaphragm Excavation Method was also slightly better than the Three-bench Excavation Method in terms of the area of the region where plastic strain occurred.

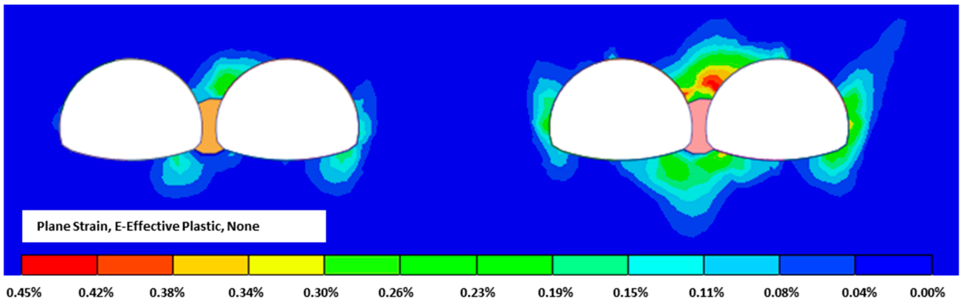

(**a**)

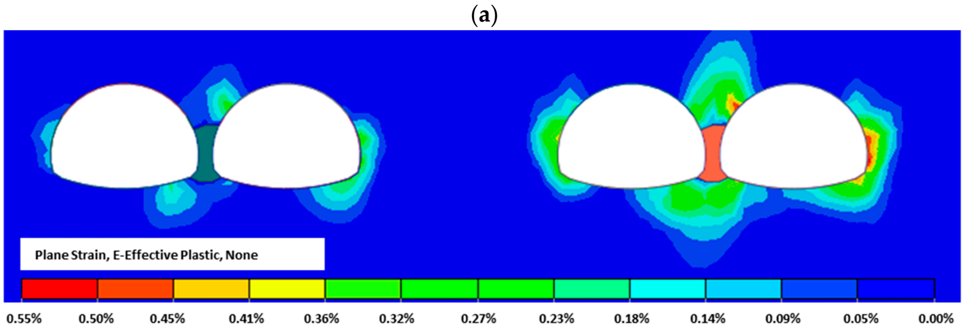

(**b**)

Figure 16. Effective plastic strain: (**a**) center Diaphragm Excavation Method; (**b**) Three-bench Excavation Method.

4.2.2. Deformation Analysis

(1) Deformation analysis of the surrounding rock and tunnel

The vertical displacement of the tunnel under the two excavation methods is shown in Figure 17. In both excavation methods, the "collapsed arch" phenomenon was observed in the surrounding rock above the tunnel. For both excavation methods, the maximum vertical settlement of the tunnel occurred at the left side of the arch top of Tunnel 4. To further study the deformation process of the tunnel under both excavation methods, the vertical displacement at this point was plotted as a graph during the excavation process, as shown in Figure 18. It was found that, when the Three-bench Excavation Method was used, the settlement of the tunnel produced a larger increase in the upper-step construction stage. When the Center Diaphragm Excavation Method was used, the settlement produced a larger growth in the upper-step construction stage of the main cavern. Compared with the Three-bench Excavation Method, the deformation process of the tunnel was smoother when the Center Diaphragm Excavation Method was adopted. This was because the Center Diaphragm Excavation Method had a smaller excavation area and was equipped with temporary support. The final settlement when using the Center Diaphragm Excavation Method was 1.33 cm, while the final settlement when using the Three-bench Excavation Method was 1.48 cm. The Center Diaphragm Excavation Method was therefore slightly better than the Three-bench Excavation Method. The settlement of both excavation methods was within a safe range.

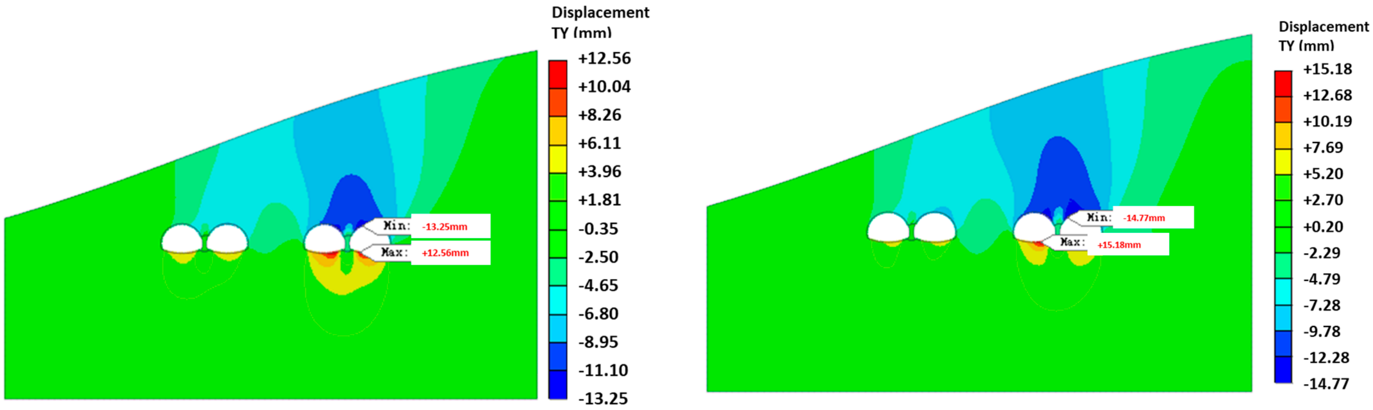

(**a**) (**b**)

Figure 17. Vertical deformation clouds under different excavation methods: (**a**) Center Diaphragm Excavation Method; (**b**) Three-bench Excavation Method.

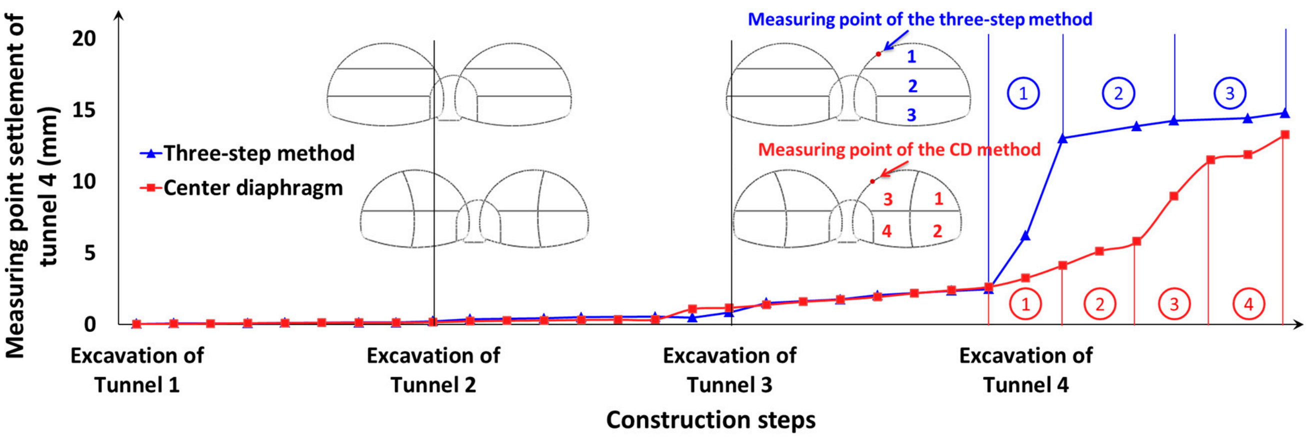

Figure 18. Deformation curve of vertical displacement of measurement points with excavation steps.

(2) Tipping analysis of the middle partition wall

The horizontal displacement of the middle partition wall under different excavation methods is shown in Figure 19. The middle partition walls under the two excavation methods were mainly deformed by tipping, and the maximum horizontal deformation occurred at the top of the middle partition wall on the shallow-buried side. The horizontal deformation of the top of the shallowly buried side of the middle partition wall under the two excavation methods was plotted in Figure 20. Regardless of the excavation method, the horizontal deformation at the top of the middle partition wall gradually increased during the construction process. Numerically, the final cumulative horizontal deformation of the diaphragm wall during excavation when using the Center Diaphragm Excavation Method and Three-bench Excavation Method was 2.85 mm and 3.79 mm, respectively. The Center Diaphragm Excavation Method was therefore slightly better than the Three-bench Excavation Method. However, it should be noted that the deformation of the middle partition wall under both excavation methods did not exceed 4 mm. Both were in a safe condition.

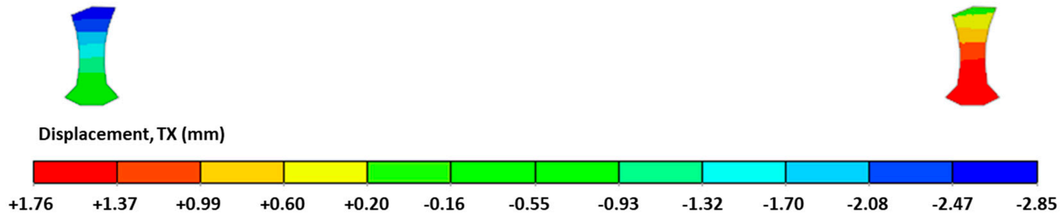

(**a**)

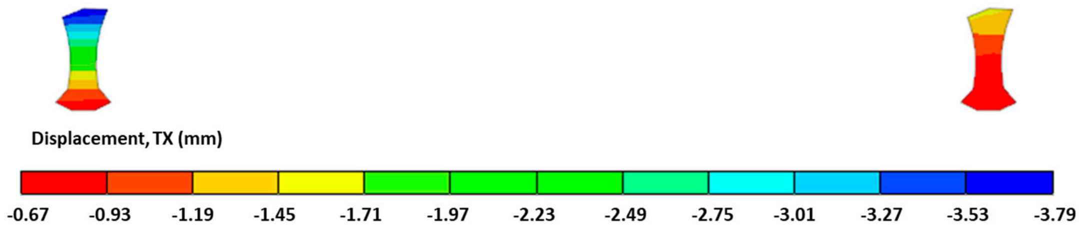

(**b**)

Figure 19. Horizontal deformation clouds of the middle partition wall under different excavation methods: (**a**) Center Diaphragm Excavation Method; (**b**) Three-bench Excavation Method.

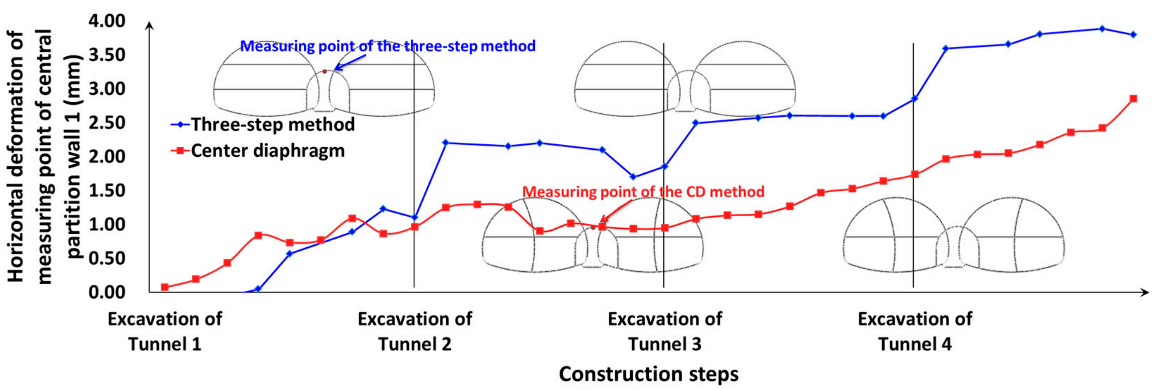

Figure 20. Horizontal deformation clouds of the middle partition wall on the shallowly buried side under different excavation methods.

4.2.3. Force Analysis

(1) Force analysis of the support structure

The initial support structure was essential for the timely reinforcement and stability of the surrounding rock during tunnel construction. As a compressive element, it was not only required to ensure that the axial force met the design requirements but also to avoid excessive local bending moments, which could have caused excessive structural deformation or even damage. Figure 21, Figure 22, and Figure 23 showed the axial force, bending moment, and shear force distribution of the initial support under the two excavation schemes, respectively. Due to the asymmetrical pressure, the internal forces of the tunnel structure exhibited an asymmetric distribution in both excavation schemes. Regarding the axial forces, as shown in Figure 21a,b, the axial forces for both excavation schemes were larger at the top, shoulder, and foot of the vault. Numerically, the maximum axial force for the Three-bench Excavation Method was 2.455 MPa, while the maximum axial force for the Center Diaphragm Excavation Method was 2.338 MPa, with little difference between them. Concerning the bending moment, both excavation schemes resulted in a larger bending moment at the arch footing area. It should be noted that, when the Center Diaphragm Excavation Method was used for the excavation, as shown in Figure 22a, a larger bending moment would be generated during the combination of the temporary support and the initial support at the arch top, which was not reasonable for the initial support structure. On the other hand, when the three-step excavation was used, as depicted in Figure 22b, a large bending moment was generated at the joint part of the middle partition wall and the arch shoulder, as the pressure of the surrounding rock was transferred to the middle partition wall through the initial support after the excavation of the upper and middle steps was completed. In terms of the final values, the absolute values of the maximum bending moment for the Center Diaphragm Excavation Method and Three-bench Excavation Method were 0.225 MPa and 0.157 MPa, respectively, indicating that the Three-bench Excavation Method was better than the Center Diaphragm Excavation Method. For the shear force, as shown in Figure 23, its distribution followed a similar pattern to that of the bending moment; therefore, further elaboration was unnecessary. The absolute values of the maximum shear force for the Center Diaphragm Excavation Method and the Three-bench Excavation Method were 0.256 MPa and 0.173 MPa, respectively, confirming that the Three-bench Excavation Method was still superior to the Center Diaphragm Excavation Method.

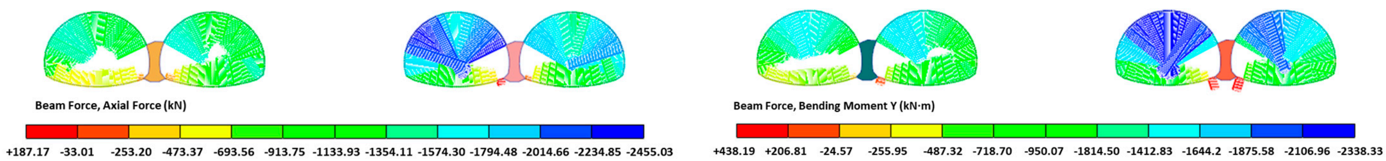

(**a**) (**b**)

Figure 21. The axial force of support structures under different excavation methods: (**a**) Center Diaphragm Excavation Method; (**b**) Three-bench Excavation Method.

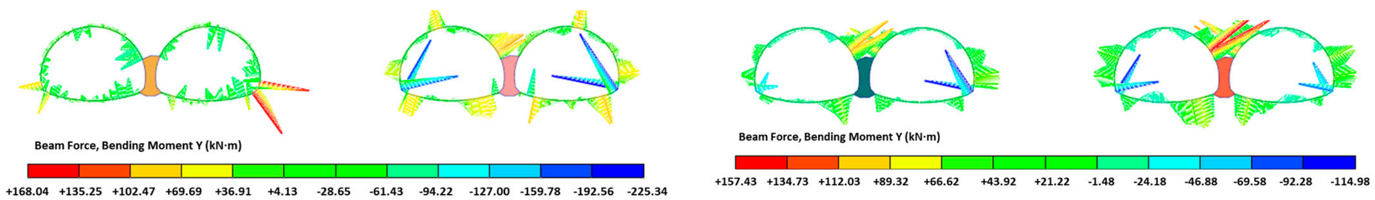

(**a**) (**b**)

Figure 22. Bending moment of support structures under different excavation methods: (**a**) Center Diaphragm Excavation Method; (**b**) Three-bench Excavation Method.

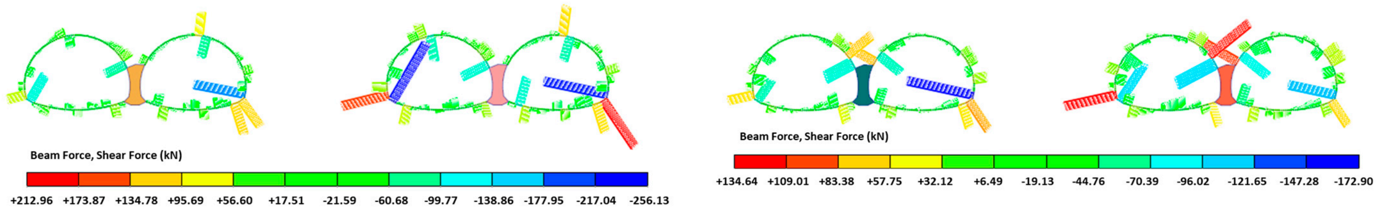

(**a**) (**b**)

Figure 23. The shear force of support structures under different excavation methods: (**a**) Center Diaphragm Excavation Method; (**b**) Three-bench Excavation Method.

(2) Stress analysis of the middle partition wall

The middle partition wall, as the key-bearing structure of the double-arch tunnel, was of utmost importance. It had to withstand not only the load from the upper rock but also the load transmitted by the lining on both sides. The burial depth of the strata, asymmetrical pressure, construction method, and construction disturbance all resulted in asymmetrical pressure in the diaphragm wall, which had a significant impact on tunnel stability. Figures 24 and 25 present the maximum and minimum principal stresses in the middle partition wall after the construction of the two excavation methods, respectively. The maximum tensile stress in the middle partition wall was 6.514 MPa for the Center Diaphragm Excavation Method and 7.070 MPa for the Three-bench Excavation Method, with the latter slightly outperforming the former. Both excavation methods exceeded the tensile strength of C35 concrete, indicating the need for the reinforced strengthening of the bottom part of the middle partition wall. Regarding the maximum compressive stress, it was 12.242 MPa for the Center Diaphragm Excavation Method and 12.480 MPa for the Three-bench Excavation Method, with a small difference between them.

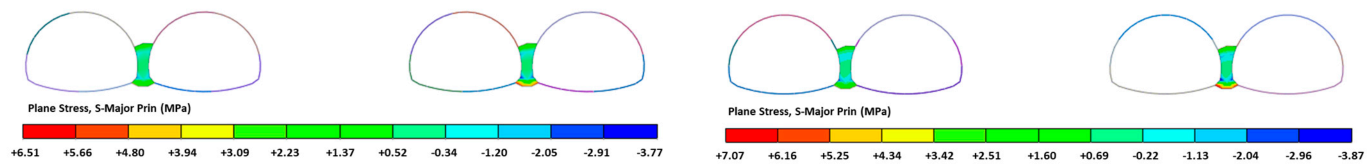

(**a**) (**b**)

Figure 24. The tensile principal stress of the central partition wall under different methods: (**a**) Center Diaphragm Excavation Method; (**b**) Three-bench Excavation Method.

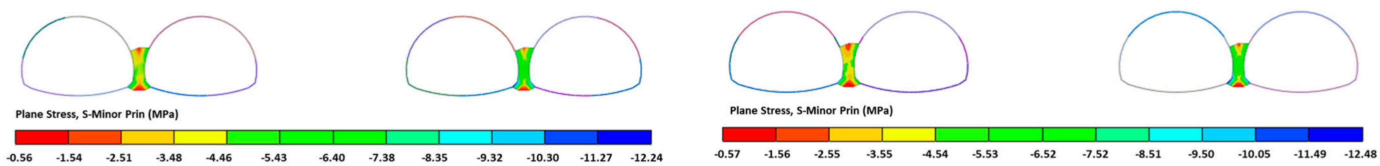

(**a**) (**b**)

Figure 25. The compressive principal stress of the central partition wall under different methods: (**a**) Center Diaphragm Excavation Method; (**b**) Three-bench Excavation Method.

4.2.4. Determination of Excavation Method

Based on the above analysis, it was observed that, in terms of surrounding rock deformation and plastic zones, the Center Diaphragm Excavation Method would be a little better.. However, the maximum surrounding rock deformation of both excavation methods fell within an allowable range. Regarding the support structure force, the Center Diaphragm Excavation Method led to a larger bending moment and shear force during the combination of the temporary support and initial support. As the Center Diaphragm Excavation Method has more excavation steps, multiple disturbances increase the force of the initial support already applied. Therefore, the initial support force of the Three-bench Excavation Method was smaller than that reported for the Center Diaphragm Excavation Method. The stress difference in the middle partition between the Center Diaphragm Excavation Method and the Three-bench Excavation Method was not significant. It is important to note that the Center Diaphragm Excavation Method required the excavation of a large number of guide holes and the erection of numerous supports to complete the construction of four lines, which could have had a detrimental effect on cost control during construction [28]. Therefore, under the conditions of this project, the Three-bench Excavation Method is the recommended choice.

4.3. Adjustment of Construction Methods

Based on the above simulation, the excavation sequence of "1→2→3→4" was selected for the construction site. At the same time, the excavation method was adjusted to the three steps method, and the pre-supporting was continued in combination with the overrunning small conduit. The top and bottom of the middle partition wall were anchored before being poured to prevent it from tipping over.

4.3.1. Adjusting the Construction Method to Three-Step Excavation Method

Before excavating using the three-stage method, the through of the two middle guide holes and the pouring of the middle partition wall had been completed. Small conduit grouting was used for over-support, as shown in Figure 26. The small conduit was made of Φ42 × 4 mm hot-rolled seamless steel pipe. Drilled Φ8 mm holes were made in the steel pipe. Then the cement slurry would be injected. The spacing of the steel pipe was 40 cm. The outer insertion angle was 12°. The tail end was supported on the steel frame. The two rows of the small conduit longitudinal laps were no less than 1 m.

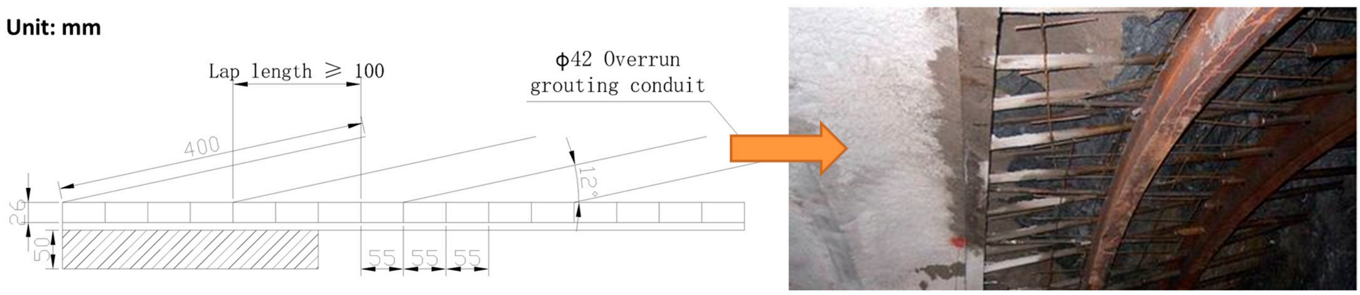

Figure 26. The Small conduit grouting for the over support before the excavation.

When using the Three-bench Excavation Method, the upper step of the tunnel is excavated and the arch top support is applied first. Next, the middle step of the tunnel is excavated, and the initial support of the middle step is applied. Next, the lower step of the tunnel is excavated, and then the initial support of the lower step is constructed. The construction process is shown in Figure 27. Finally, the secondary lining was poured and the backfill of the inverted arch was carried out. After the strength of the secondary lining reached the design requirements, the other side was excavated.

4.3.2. Anchoring of the Middle Partition Wall

The numerical simulation results showed that the middle partition wall was prone to tipping deformation. The site personnel used anchors to reinforce the top and bottom of the middle partition wall before it was applied, as shown in Figure 28.

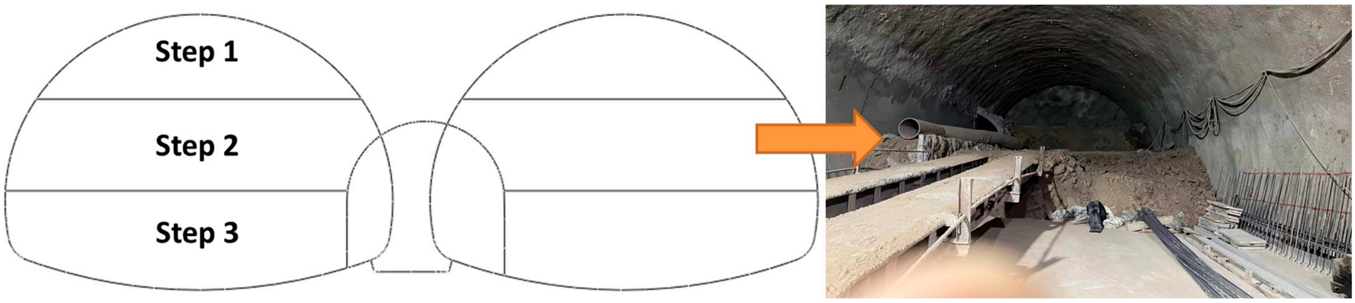

Figure 27. The excavation using the Three-bench Excavation Method.

Figure 28. The anchoring at the top and bottom of the middle partition wall.

5. Conclusions

The excavation sequence and excavation method of the Wengcun Tunnel of Guangxi G72 project were examined using numerical simulation in the background. Based on the numerical simulation, the on-site construction method was adjusted. The following conclusions were obtained:

(1) Under the asymmetrical load, the deformation and force of the surrounding rock were greater on the deeply buried side. The tipping deformation of both middle partition walls was toward the shallow side. The tipping magnitude of the middle partition wall on the shallow side was greater;
(2) The effect of the excavation sequence on horizontal deformation was greater than that of vertical deformation. If the shallow side is excavated first, the asymmetric load generated by the construction and the topography are opposite. This was more conducive to the safety of the tunnel;
(3) In this project, the mutual influence generated by the construction of the left line and the right line was not significant. Therefore, the excavation sequence of either "1→2→3→4" or "3→4→1→2" was feasible;
(4) In terms of the surrounding rock deformation and plastic zone, the Center Diaphragm Excavation Method was slightly better than the Three-bench Excavation Method. In terms of the support structure force, the Center Diaphragm Excavation Method was slightly inferior to the Three-bench Excavation Method;
(5) The index difference between the Center Diaphragm Excavation Method and the Three-bench Excavation Method was not large, and the settlement of the vault was 1.33 cm and 1.48 cm, respectively, which is within a safe range. The Three-bench Excavation Method is more economical; therefore, it is recommended;
(6) Based on the numerical simulation results, the construction sequence of the shallow-buried side of the tunnel first was adopted in the actual construction process. The

excavation method was adjusted to the Three-bench Excavation Method. The top and bottom of the middle partition wall were reinforced with anchors.

Author Contributions: S.W. carried out the main research task and wrote the manuscript. D.L. proposed the original idea and contributed to the revision of the obtained results and the whole manuscript. J.W. was a mentor outside of the school. He proposed the method of tunnel construction for the engineering conditions at the site, which was critical for this project. All authors have read and agreed to the published version of the manuscript.

Funding: This research received no external funding.

Data Availability Statement: The data presented in this study are available on request from the corresponding author.

Acknowledgments: The authors would like to acknowledge Road and Bridge South China Engineering for providing detailed information about the design and construction. Meanwhile, the authors would like to express their gratitude to Yunchuan Zhang for his help during the field investigation.

Conflicts of Interest: The authors declare no conflict of interest.

References

1. Jiang, Q.; Song, S.-G.; Li, T.; Wang, K.; Gu, R.-H. Study on Surrounding Rock Stability of Small Clear-Distance Twin Highway Tunnel with Eight Lanes. *Geotech. Geol. Eng.* **2019**, *37*, 593–598. [CrossRef]
2. Li, R.; Chen, P.; Zhang, D.L.; Wang, S.T.; Shen, Z.J.; Pan, H.G. Numerical study and engineering practice for surrounding rock stability of large cross-sectional triple tunnels. *China Civ. Eng. J.* **2022**, *55*, 83–95. [CrossRef]
3. Xue, Y.; Gong, H.; Kong, F.; Yang, W.; Qiu, D.; Zhou, B. Stability analysis and optimization of excavation method of double-arch tunnel with an extra-large span based on numerical investigation. *Front. Struct. Civ. Eng.* **2021**, *15*, 136–146. [CrossRef]
4. Wang, J.; Cao, A.; Wu, Z.; Sun, Z.; Lin, X.; Sun, L.; Liu, X.; Li, H.; Sun, Y. Numerical Simulation of Ultra-Shallow Buried Large-Span Double-Arch Tunnel Excavated under an Expressway. *Appl. Sci.* **2022**, *12*, 39. [CrossRef]
5. Fu, J.; Yang, J.; Yan, L.; Abbas, S.M. An analytical solution for deforming twin-parallel tunnels in an elastic half plane. *Int. J. Numer. Anal. Methods Geomech.* **2015**, *39*, 524–538. [CrossRef]
6. Li, G.J.; Zhai, Y.; Lu, G.S.; Liu, J.S. Surrounding Rock Pressure of Tunnel with Small Clear Distance under Complex Unsymmetrical Loading: Calculation and Parameter Impacts. *J. Yangtze River Sci. Res. Inst.* **2020**, *37*, 133–138.
7. Yang, S.; Dai, R.; Ai, Z.; Li, X.; Zhang, C.; Huang, X. Analytical Solutions for the Mechanical Responses of Shallow Double-Arched Tunnel Subjected to Symmetric Loads. *Adv. Civ. Eng.* **2021**, *2021*, 8867536. [CrossRef]
8. Hu, X.; Zhang, Z.; Teng, L. An analytical method for internal forces in DOT shield-driven tunnel. *Tunn. Undergr. Space Technol.* **2009**, *24*, 675–688. [CrossRef]
9. Yao, Y.; He, C.; Zhang, L.L. Experimental Study of Site Monitoring of Zipingpu Tunnel with Small Clear Spacing. *Chin. J. Rock Mech. Eng.* **2010**, *29*, 3295–3300.
10. Wu, J.M.; Chen, X.C.; Li, W.Q.; Peng, J.Z.; Zhang, A.L. Forecast of overbreak and analysis of cause of formation in double-arch tunnels in Jinliwen highway. *Hydrogeol. Eng. Geol.* **2005**, *32*, 56–59. [CrossRef]
11. Yan, Q.; Zhang, C.; Lin, G.; Wang, B. Field Monitoring of Deformations and Internal Forces of Surrounding Rocks and Lining Structures in the Construction of the Gangkou Double-Arched Tunnel—A Case Study. *Appl. Sci.* **2017**, *7*, 169. [CrossRef]
12. Lai, J.; Qiu, J.; Fan, H.; Chen, J.; Hu, Z.; Zhang, Q.; Wang, J. Structural Safety Assessment of Existing Multiarch Tunnel: A Case Study. *Adv. Mater. Sci. Eng.* **2017**, *2017*, 1697041. [CrossRef]
13. Yuan, Y.; Wang, S.H.; Du, G.P.; Li, D. In-Situ Testing Study on Lining System of doubleArched Tunnel. *Chin. J. Rock Mech. Eng.* **2005**, *24*, 480–484.
14. Lei, M.-F.; Lin, D.-Y.; Yang, W.-C.; Shi, C.-H.; Peng, L.-M.; Huang, J. Model test to investigate failure mechanism and loading characteristics of shallow-bias tunnels with small clear distance. *J. Cent. South Univ.* **2016**, *23*, 3312–3321. [CrossRef]
15. Jiang, X.L.; Wang, F.F.; Yang, H.; Lian, P.Y.; Niu, J.Y. Study on Seismic Lining Strain Law of Shallow-buried Bias Tunnel with Small Clear Distance. *Chin. J. Undergr. Space Eng.* **2017**, *13*, 506–516.
16. Li, S.; Yuan, C.; Feng, X.; Li, S. Mechanical behaviour of a large-span double-arch tunnel. *KSCE J. Civ. Eng.* **2016**, *20*, 2737–2745. [CrossRef]
17. Yang, J.S.; Gou, D.M.; Zhang, Y.X. Field Measurements and Numerical Analyses of Double-Layer Pipe Roof Reinforcement in a Shallow Multiarch Tunnel. *Transp. Res. Rec.* **2008**, *2050*, 145–153. [CrossRef]
18. Liu, X.R.; Liu, J.; Huang, L.H.; Wang, Z.J.; Chen, H.J.; Feng, Y. Model test and pressure arch analysis for excavation of loess double arch tunnel. *J. Zhejiang Univ. Eng. Sci.* **2018**, *52*, 1140–1149.
19. Wang, J.; Cao, A.; Li, Z.; Wu, Z.; Lin, L.; Liu, X.; Li, H.; Sun, Y. Mechanical Behavior and Excavation Optimization of a Small Clear-Distance Tunnel in an Urban Super Large and Complex Underground Interchange Hub. *Appl. Sci.* **2023**, *13*, 254. [CrossRef]

20. Ng, C.W.; Lee, K.M.; Tang, D.K. Three-dimensional numerical investigations of new Austrian tunnelling method (NATM) twin tunnel interactions. *Can. Geotech. J.* **2004**, *41*, 523–539. [CrossRef]
21. Zhang, Y.L.; Fu, X.K.; Liu, H.L.; Zheng, Y.Y. Study on the reasonable excavation sequence of shallow-embedded bias tunnels with small clear distance. *J. Railw. Eng. Soc.* **2013**, *10*, 57–63. [CrossRef]
22. Xu, Q.; Xu, W.; Li, P.; Liu, Y. A Hybrid Construction Method for Shallow Buried Urban Tunnel with Ultra-Small Clear Distance. *IOP Conf. Ser. Mater. Sci. Eng.* **2020**, *960*, 032007. [CrossRef]
23. Soliman, E.; Duddeck, H.; Ahrens, H. Two- and three-dimensional analysis of closely spaced double-tube tunnels. *Tunn. Undergr. Space Technol.* **1993**, *8*, 13–18. [CrossRef]
24. Bai, J.S.; Zhao, S.P.; Qi, B.; Yang, K.F. Study on the structure deformation of large-span shallow-buried multi-arch tunnel in soft stratum. *China Civ. Eng. J.* **2017**, *50*, 45–50. [CrossRef]
25. Yao, A.; Lin, J.; Ren, B. The Influence of Small Clear-Distance Tunnel Construction on Adjacent High-Voltage Transmission Tower Foundation. *Adv. Civ. Eng.* **2023**, *2023*, 2533212. [CrossRef]
26. Qi, H.; Gao, B.; Wang, S.S.; Xu, C. Mechanical Behaviors of a Shallow-Bias Tunnel with a Small Clear Distance in Different Geological Conditions. *Mod. Tunn. Technol.* **2014**, *51*, 108–112. [CrossRef]
27. Zhao, J.P.; Wang, X.Y.; Tan, Z.S.; Zhang, C.; Wang, Z.X. Study on the reasonable construction layout of main tunnel in unsymmetrical loading multi-arch tunnel with weak rock. *China Civ. Eng. J.* **2017**, *50*, 66–74. [CrossRef]
28. Zhang, F. Stability Analysis of Construction Process of New Tunnel Passing through High-speed Railway Foundation. *J. Railw. Eng. Soc.* **2022**, *39*, 53–58+79.